LA-UR-18-29076
Approved for public release; distribution is unlimited.

Title: Advanced Integration of High Dose Neutron, Microcalorimeter and Voltammetry Sensor Technologies in an Electro-Refining Process

Author(s): Tutt, James Robert
Fugate, Michael Lynn
Key, Brian P.

Intended for: Report

Issued: 2018-09-24

Advanced Integration of High Dose Neutron, Microcalorimeter and Voltammetry Sensor Technologies in an Electro-Refining Process

James Tutt, Mike Fugate, and Brian Key

Los Alamos National Laboratory

September 28, 2018

1 Introduction

In this report we examine measurements from two different sensors, for detecting a diversion of plutonium in an electro-refining (ER) process. One method is based on counts from a high dose neutron detector (HDND). The other is based on spectra from a micro-calorimeter sensor. The spectra comes from the ER-salt, from fission product waste and from a source term. The goal is to differentiate between normal and off normal operating conditions using neutron counts or changes in counts in the spectra. Unfortunately, there is no electro-refining process that we can actually monitor to obtain real data from various operating conditions so we will use simulated data to illustrate our approach. The data used to simulate the performance of the HDND and the microcalorimeter was provided by the Separations and Safeguards Performance Model (SSPM) [1]. The SSPM EChem software tracks material flows and mass inventories through each unit operation of an electrochemical reprocessing plant. In mid-May the advanced integration team received a mass inventory data set for each unit operation within SSPM. The data provided masses for each element 1-99 in the periodic table and was reported in hourly increments out to one operational year (6480 hours). Isotopic ratios, though tracked separately in SSPM, were also provided for each unit process on an hourly basis for 266 nuclides. Isotopic mass compositions were created by combining the elemental mass data with the isotopic ratios for each unit process. This enabled the development of realistic neutron and gamma source terms that could be distributed to technology development groups enabling deeper evaluation of detection performance.

2 Simulation of the HDND

Neutron source terms were generated from the isotopic mass concentrations for the uranium (U) and uranium-transuranic (U/TRU) products to enable simulations of the High-Dose Neutron Detector (HDND) response. The SOURCES 4C code, developed at LANL to calculate energy dependent alpha-n, spontaneous fission, and delayed neutron sources and spectra [2], was used to generate the source terms. A python script was written to convert the raw SSPM mass data into a SOURCES 4C input tape, then read the output and print the neutron energy spectrum to a text file. Automation of this process allowed the generation of neutron source terms for a variety of cases with general ease.

Several possible scenarios were considered and neutron source terms were generated for each case. The cases included steady-state masses of radionuclides in the U and U/TRU product, a diversion of 1% of the plutonium mass from the U/TRU product into the U product, and a diversion of 1% of the full U/TRU product mass into the U product. The strongest source of neutrons in the U/TRU product is curium, as shown in Tables 1 and 2. During normal operation plutonium and curium remain comingled. However, it may be feasible to separate the plutonium from the curium in a diversion scenario, drastically reducing the neutron signal of the diverted material. Therefore, cases were chosen to enable the establishment of a baseline count-rate in the HDND under normal operating conditions, then look at the response to a diversion in which the plutonium and curium are comingled vs separated.

Table 1. Neutron emissions from selected radionuclides in the U Product ingot.

U Product			
Source	Normal	1% Pu	1% U/TRU
Nuclide	(n/s-cm3)	(n/s-cm3)	(n/s-cm3)
U-238	0.254	0.254	0.254
Pu-238	0.000	0.169	0.169
Pu-240	0.001	0.653	0.653
Pu-242	0.000	0.342	0.342
Cm-244	0.072	0.072	83.35
Cm-246	0.003	0.003	3.369
Total	0.330	1.493	88.42

Table 2. Neutron emissions from selected radionuclides in the U/TRU Product ingot.

U/TRU Product			
Source	Normal	1% Pu	1% U/TRU
Nuclide	(n/s-cm3)	(n/s-cm3)	(n/s-cm3)
U-238	0.16	0.15	0.15
Pu-238	473	444	444
Pu-240	1828	1719	1719
Pu-242	957	899	899
Cm-244	233300	221500	219300
Cm-246	9431	8954	8864
Total	246800	234300	232000

Radiation transport simulations were carried out with MCNP6.2 [3] using the source terms developed from the SSPM U, and U/TRU product mass data and a detailed model of the detector provided by the HDND team. The exact dimensions of the U and U/TRU ingots are not known however the mass, density (assumed uranium metal, 18.9 g/cm^3), and therefore volume are known. Approximate

dimensions were chosen to preserve the total mass in each ingot, 72x16x16 cm and 14x7x7 cm respectively. The center of each ingot was placed 20 inches from the face of the detector in simulations.

The HDND is comprised of parallel plates of gas-proportional counters lined with boron-10. Neutrons are detected via the $^{10}B(n,\alpha)^{7}Li$ reaction whereby a pulse is produced in the detector when a neutron is captured in the boron lining and the subsequent reaction products deposit some or all of their energy in the counting gas. The HDND team had previously developed an MCNP model that simulated the response of the detector for design optimization. This model was used to find the response of the detector to the neutron source from each of the cases described above. The results of the model are shown in Table 3 and represent the number of neutron reactions that deposit enough energy in the counting gas to produce a pulse. Efficiency effects of the signal processing electronics are not included in the model.

Table 3. Pulse rate produced in detector.

Ingot	**Normal**	**1% Pu**	**1% U/TRU**
	pulses/s	pulses/s	Pulses/s
U Product	7.93	36.76	2192.6
U/TRU Product	66098.1	63992.4	64311.5

Most materials that emit neutrons also emit gamma rays which can deposit their energy in the counting gas of a detector and register a pulse, just as a neutron would, producing a 'fake' neutron count. In high gamma radiation fields this can make accurate neutron counting difficult or impossible. One of the ways the HDND can become less sensitive to gamma rays is by reducing the high voltage setting, effectively increasing the amount of required energy deposited to generate a pulse. Operating at a reduced high voltage setting greatly decreases the detector's sensitivity to gamma rays, however the neutron efficiency is also somewhat lowered.

Gamma dose rate calculations were performed with MCNP6.2 for the U/TRU ingot in order to understand how the gamma rays emitted from the ingot would affect the neutron counting efficiency of the HDND. Based on the SSPM mass data, the full U/TRU ingot (13 kg) has an activity of ~20,000 curies. The spontaneous decay feature within MCNP [4] was used to generate the delayed-gamma spectrum from the U/TRU ingot then transport those gammas in the problem. The resultant dose rate from gammas at the face of the detector (20 in from ingot) was calculated to be ~3 rem/hr. The HDND has demonstrated capability to operate at much higher gamma background environments [5] therefore the effect on neutron detection efficiency at these dose rates is expected to small.

3 Statistical Detection of Off Normal Conditions Using a HDND

In this section we consider a statistical approach for detecting a diversion of Pu by counting neutrons with a HDND. We consider process monitoring for a pure uranium product and for a U/TRU product as discussed in the last section.

Under normal conditions and no background, we expect the neutron count rate from a uranium ingot to be about 7.9 pulses/sec. If 1% of the plutonium mass from the U/TRU product is diverted to the ingot we expect the count rate to be about 36.8 pulses/sec.

For the U/TRU product, under normal operating conditions and no background, we expect the count rate to be about 66098.1 pulses/sec and if 1% of the Pu mass is diverted we expect the count rate to be about 64640.4 pulses/sec.

3.1 Detecting Diversion for U Product

For the remainder of this section consider just the case of the uranium ingot. If we monitor the process with a HDND for say, 5 minutes, the mean count rates for normal operation and 1% Pu diversion are 2370 pulses/300sec and 11040 pulses/300sec, respectively. If counts can be modeled by a Poisson distribution the standard deviation of counts is the square root of 2370 or about 49 pulses/300sec (assuming no diversion and a 5 minute count time). Clearly, if we observe counts on the order of 11040 in a 5 minute interval we have observed something quite unusual; 11040 is about 178 standard deviations above the no diversion mean of 2370. If neutron counts can be modeled reasonably well by a Poisson distribution the discussion in the previous paragraph suggest using the statistic:

$$Z = \frac{observed - expected}{\sqrt{expected}}$$

to detect a difference in counts. Here "expected" is the no diversion mean count rate and "observed" is the measured count rate. If there is a diversion of Pu the observed count rate will be larger than what is expected under normal operation and the observed value of *Z* will be large. To quantify what constitutes a large observed count we need to know the distribution of *Z* when there is no diversion.

For the examples we consider in this report if there is no diversion and the count time is at least 5 minutes, standard statistical theory can be used to show that *Z* will have an approximate (standard) Gaussian distribution with mean 0 and variance 1. Quantiles of the standard Gaussian can be used to set a threshold to distinguish between typical no diversion count rates and unusual count rates. Choosing a particular threshold determines a process monitoring false alarm rate. For example, the 95th quantile of the standard Gaussian is 1.645. If we choose 1.645 as the threshold and there is no diversion, then 95% of the time *Z* will be less than 1.645 and 5% of the time *Z* we be greater than the threshold, which implies that 5% is the false alarm rate.

For the example above with a 5 minute count time and a 1% diversion of Pu, on average

Z will be:

$$Z = \frac{(5 * 60 * 36.8) - (5 * 60 * 7.9)}{\sqrt{5 * 60 * 7.9}}$$

$$= \sqrt{300} * \frac{(36.8 - 7.9)}{\sqrt{7.9}} \approx 178$$

A value of 178 is highly unusual if there is no diversion (the 99.999th quantile of a standard Gaussian is about 4.26). Either we observed something extremely rare or there was a diversion. Note that the last equation above shows how count times influence *Z* and ultimately the probability of detection. For count time *T* we have:

$$Z = \frac{\sqrt{T}(observed - expected)}{\sqrt{expected}}.$$

Clearly, as count time increases the ability to detect a difference between observed and expected counts increases.

The above discussion considered only the case of a 1% diversion and no background noise. More generally, we would like to know the probability of detection for different diversion amounts and also what effect background has on the probability of detection.

Ideally, to estimate the probability of detection, we would actually perform many physical experiments where Pu was diverted in the electro-refining process, count the neutrons and see how often *Z* detected a significant difference. As this is not possible we will use simulations to estimate the probability of detection for various count rates and different backgrounds.

3.2 Estimated Probability of Detection

In this section we describe the algorithm used to estimate the probability of detection (PD) for various diversion count rates and background rates. For the uranium product, any diversion of Pu will lead to an increase in the count rate. For the U/TRU product a diversion of Pu will lead to a decrease in the count rate.

The following lists give the parameters that need to be set for each simulation and the steps involved in estimating the PD. In the results presented below we used three different backgrounds for the U product and three for the U/TRU product.

Parameters Set by User:

- *Q* quantile from standard Gaussian distribution that determines the false alarm rate (e.g. choose 1.645 for a 5% false alarm rate)
- S_0 the mean count rate for normal operating conditions (either 7.9 or 66098.1 pulses/sec)
- S_1 the mean count rate when some amount of Pu has been diverted (pulses/sec)

- B the mean count rate for the background (pulses/sec)
- T the time to count neutrons in seconds (we used 300 and 600)

Simulation Steps:

1. $\mu_0 = (S_0 + B)T$, the no diversion mean count rate in a unit of time T
2. $\mu_1 = (S_1 + B)T$, the diversion mean count rate in a unit of time T
3. Simulate N pseudo-random Poisson counts with mean μ_1. Let w_i be the observed count from simulation i, for $i = 1, \ldots, N$ (we used $N = 100000$)
4. Calculate $Z_i = (w_i - \mu_0)/\sqrt{\mu_0}$, for $i = 1, \ldots, N$
5. Estimate the probability of detection (PD) as the fraction of times Z_i is greater than the threshold Q
6. Note, if $\mu_1 = \mu_0$ the PD should be very close to the false alarm rate with any difference due to simulation error. As N gets large this error should approach 0.

In the following sections we show probability of detection rates for the U and U/TRU products. Because the two products have very different mean count rates the simulation parameters need to be quite different.

4 U Product

This section shows estimated probability of detection for the U product. Recall that a 1% diversion of Pu will result in a count rate of 36.8 pulses/sec, which is quite easy to detect, even in the presence of significant background noise. To make results a little more interesting we decided to use diversion count rates from 8 to 9 pulses/sec. The following list shows the parameters of the simulation.

- Normal (no diversion) count rate: 7.9 pulses/sec
- Background: none, 100% of normal (or 7.9 pulses/sec) and 200% of normal (or 15.8 pulses/sec)
- Diversion count rates (pusles/sec): 10 equally spaced values from 7.9 to 9. Note that 7.9 corresponds to no diversion.
- Count time: 5 and 10 minutes
- False alarm rate: 5%
- Number of simulations: 100000

Figure 1 shows the probability of detection for the various scenarios plotted as a function of the no background count rates. The dashed curves correspond to 5 minute count times and the solid curves correspond to 10 minute count times. Curves of the same color have the same background count rate.

Comparing two curves of the same color shows that the PD is higher for longer count times. Comparing solid curves of different colors or dashed curves of different colors shows that the PD is higher for lower background counts. As expected, higher count times and lower backgrounds result in higher PD. Note that the dashed blue curve and the red solid curve are essentially the same. This says that counting for 5 minutes with no background (dashed blue) gives the same PD as counting for 10 minutes when background is 7.9 pulses/sec (solid red) which is a coincidence of the parameters used in the simulations.

Each circle on a curve is a PD for a particular simulation scenario. The PD is estimated by counting how many times the statistic *Z* exceeds some threshold. Figure 2 shows a histogram of all the values for one scenario. This particular scenario has a 10 minute count time and a diversion count rate with no background of 8.14 pulses/sec. Every point on every curve in Figure 1 has a similar histogram.

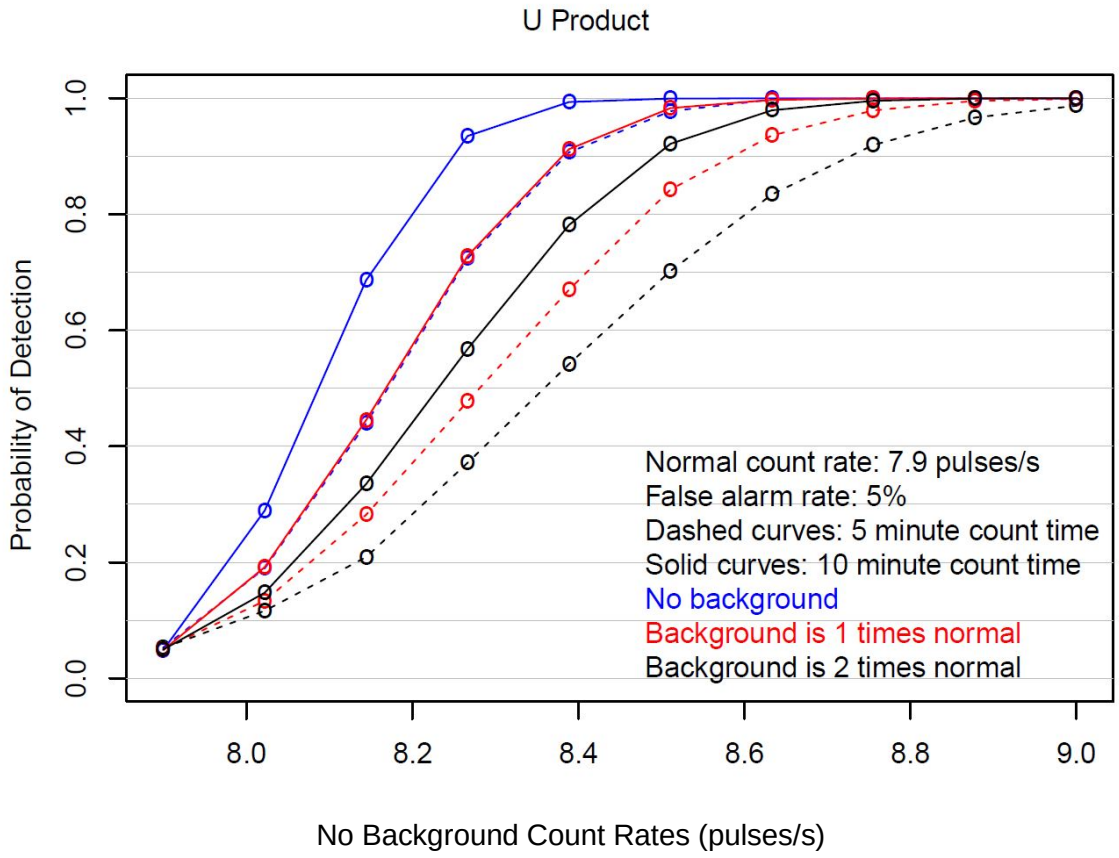

Figure 1: Probability of detection for various count rates, times, and backgrounds. Curves of the same color have the same background count rate. Note that the dashed blue curve plots under the solid red curve.

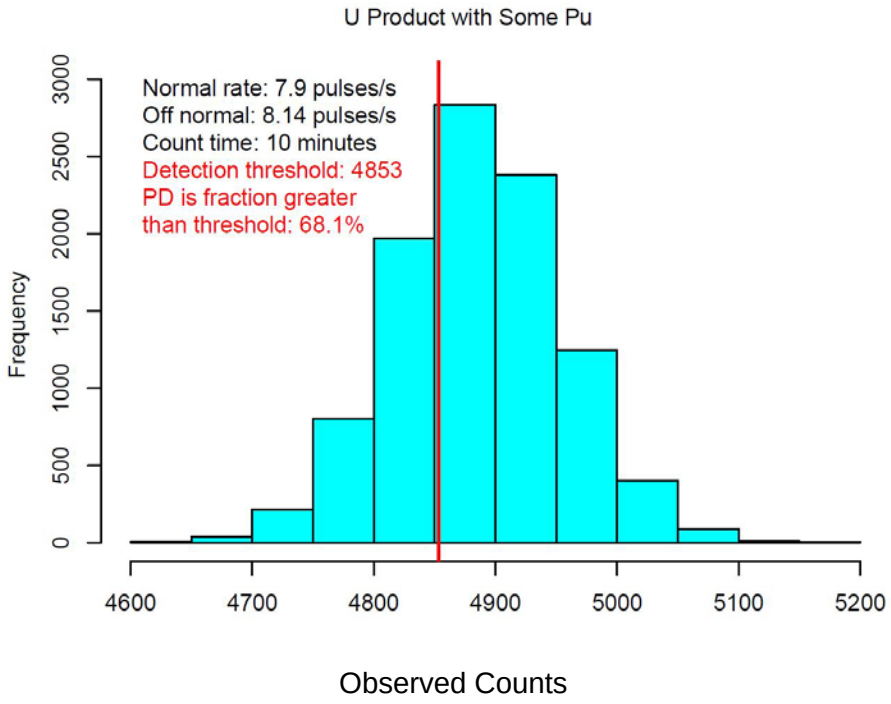

Figure 2: Observed counts for one off normal rate and no background. Compare to the third circle on the solid blue curve in the previous figure.

5 U/TRU Product

This section shows estimated probability of detection for the U/TRU product. Recall that a 1% diversion of Pu will result in a count rate of 64640.4 pulses/sec, which is quite easy to detect, even in the presence of significant background noise. Because count rates are so high relatively small difference in rates can be detected quite easily. Because of this we decided to examine what effect very high background rates have on the PD. The following list shows the parameters of the simulation.

- Normal (no diversion) count rate: 66098.1 pulses/sec
- Background: none, 20 *times* normal and 50 *times* normal
- Diversion count rates (pusles/sec): 10 equally spaced values from 64640.4 to 66098.1. Note that 66098.1 corresponds to no diversion.
- Count time: 5 and 10 minutes
- False alarm rate: 5%
- Number of simulations: 100000

Figure 3 shows the probability of detection for the various scenarios plotted as a function of the no background count rates. The dashed curves correspond to 5 minute count times and the solid curves correspond to 10 minute count times. Curves of the same color have the same background count rate.

The reason background rates have to be so high to see some difference in PD is because, with Poisson data, the standard deviation is the square root of the mean and, compared to the mean, the square root of the mean is relatively small when counts are large. Also, if we look at the form of the *Z* statistic we can see just how unusual a count of 64640.4 is relative to the no diversion mean count rate of 66098.1

$$Z = \frac{(66098.1 - 64640.4)}{\sqrt{66098.1}} \approx 5.7$$

In other words, a count rate of 64640.4 is about 5.7 standard deviations from the mean rate of 66098.1. So, if we count for even a small amount of time the difference becomes highly significant. For example, if we count for 5 minutes the *Z* value is $\sqrt{300}(5.7)$, or about 98 standard deviations from the no diversion mean. Continuing further, if the background rate is *X* times the no diversion rate and the count time in seconds is *T*, then on average we will have

$$Z = \frac{\sqrt{T}((X+1)expected - \big(observed + X(expected)\big))}{\sqrt{(X+1)expected}}$$

$$= \frac{\sqrt{T}(expected - observed)}{\sqrt{X+1}\sqrt{expected}}.$$

If there is no background then *X* is 0 and this is the *Z* statistic above (with observed and expected switched in the numerator). The last line shows the benefit of long count times.

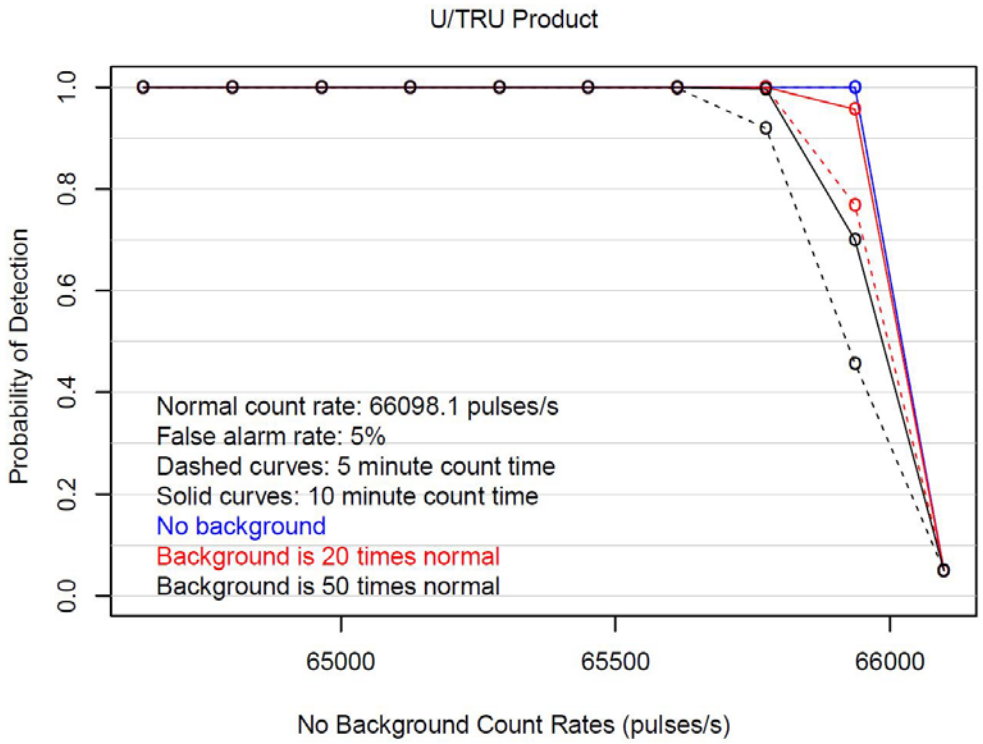

Figure 3: Probability of detection for various count rates, times, and backgrounds. Curves of the same color have the same background count rate. Note that the dashed blue curve plots under the solid red curve.

6 Simulation of the Microcalorimeter

The mircrocalorimeter has been identified as a technology that can provide remarkably higher energy resolution than other such instruments for gamma spectroscopy such as HPGe [6]. The following sections detail new information regarding the performance of the microcalorimeter given new data. For details on how the microcalorimeter is modeled and PD's determined, the reader is encouraged to read the previous report [7]. Gamma source terms were created from the SSPM mass data using the Intrinsic Source Constructor (ISC) code [8] at several locations to evaluate the microcalorimeter response to each of these materials. Locations evaluated were the source term, ER salt, and fission product waste. The gamma source terms for each of these locations were then used to simulate the microcalorimeter response in GEANT4 [9]. Figure 4 shows a microcalorimeter spectrum generated from the ER salt gamma source term. The five largest peaks belong to Am-241, Eu-154, Eu-155, and Pb-212.

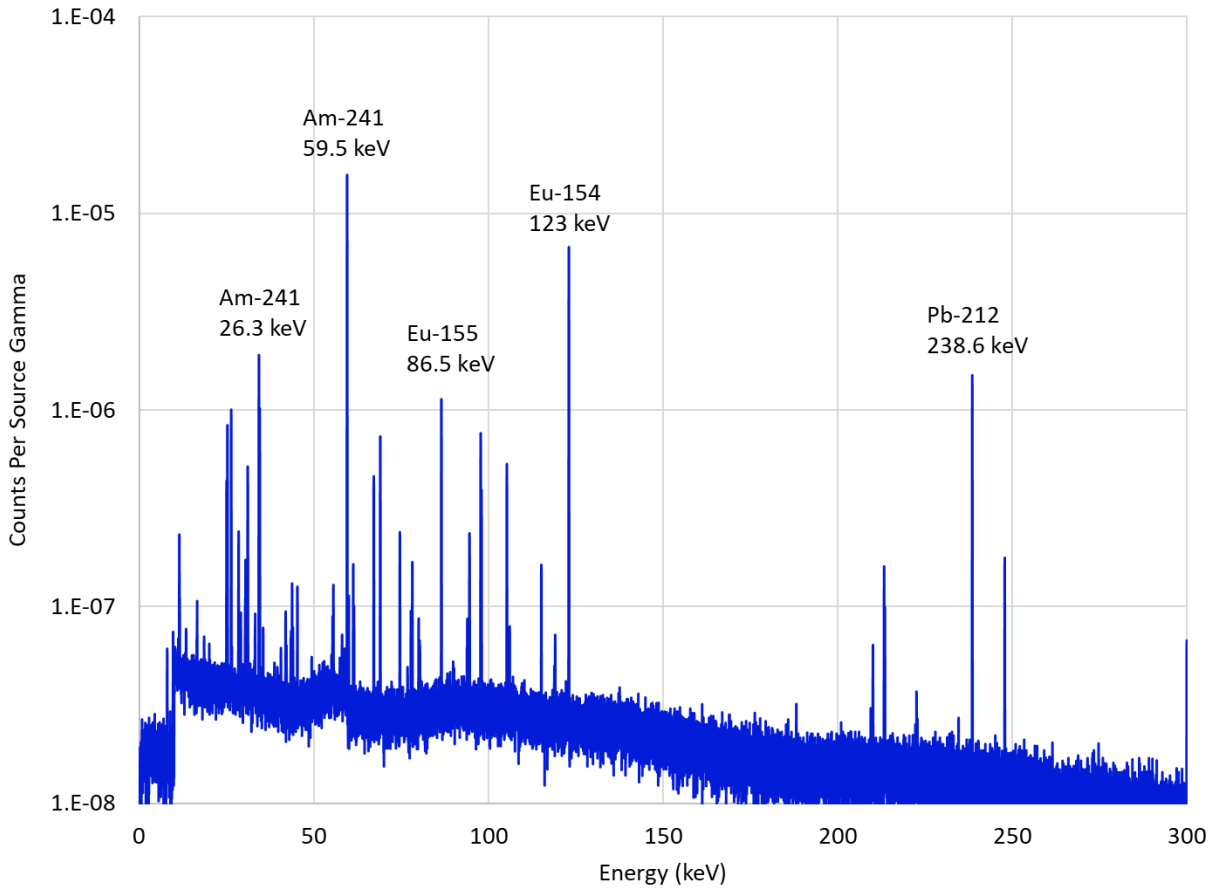

Figure 4: Microcalorimeter spectrum generated from ER salt gamma source term.

7 Microcalorimeter Spectra for ER-Salt

This section looks at detecting a diversion in the ER-salt based on spectra of counts from the microcalorimeter sensor. Figure 5 shows four high intensity gamma lines that correspond to isotopes we used in a previous study. Figure 6 shows detection probabilities for a 5% false positive rate when 1% and 1.5% Pu is diverted. Because counts are so high we only used the Eu-155 peak at 105.31 keV.

The methodology for generating the PD's shown in Figure 6 for the microcalorimeter are detailed in the previous advanced integration report [7]. The reader is invited to review that report to discover modeling details of the microcalorimeter.

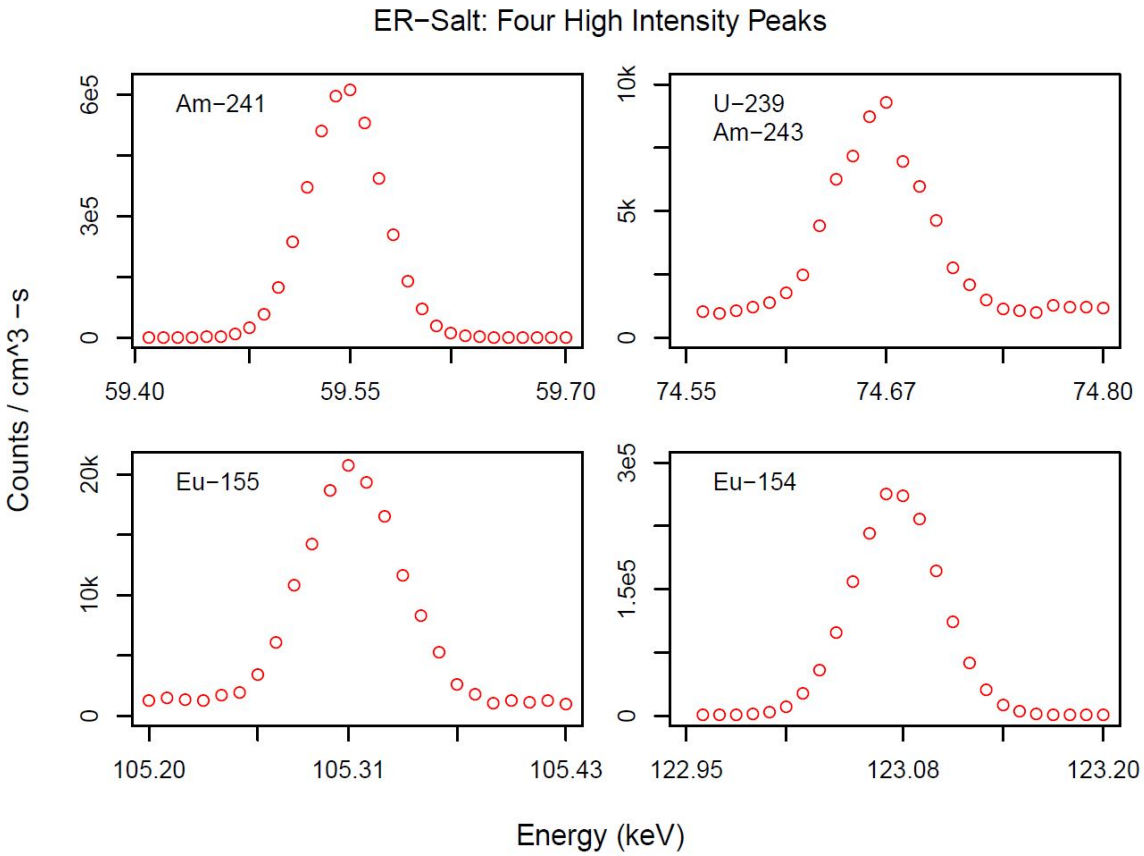

Figure 5: ER-salt isotopes of interest.

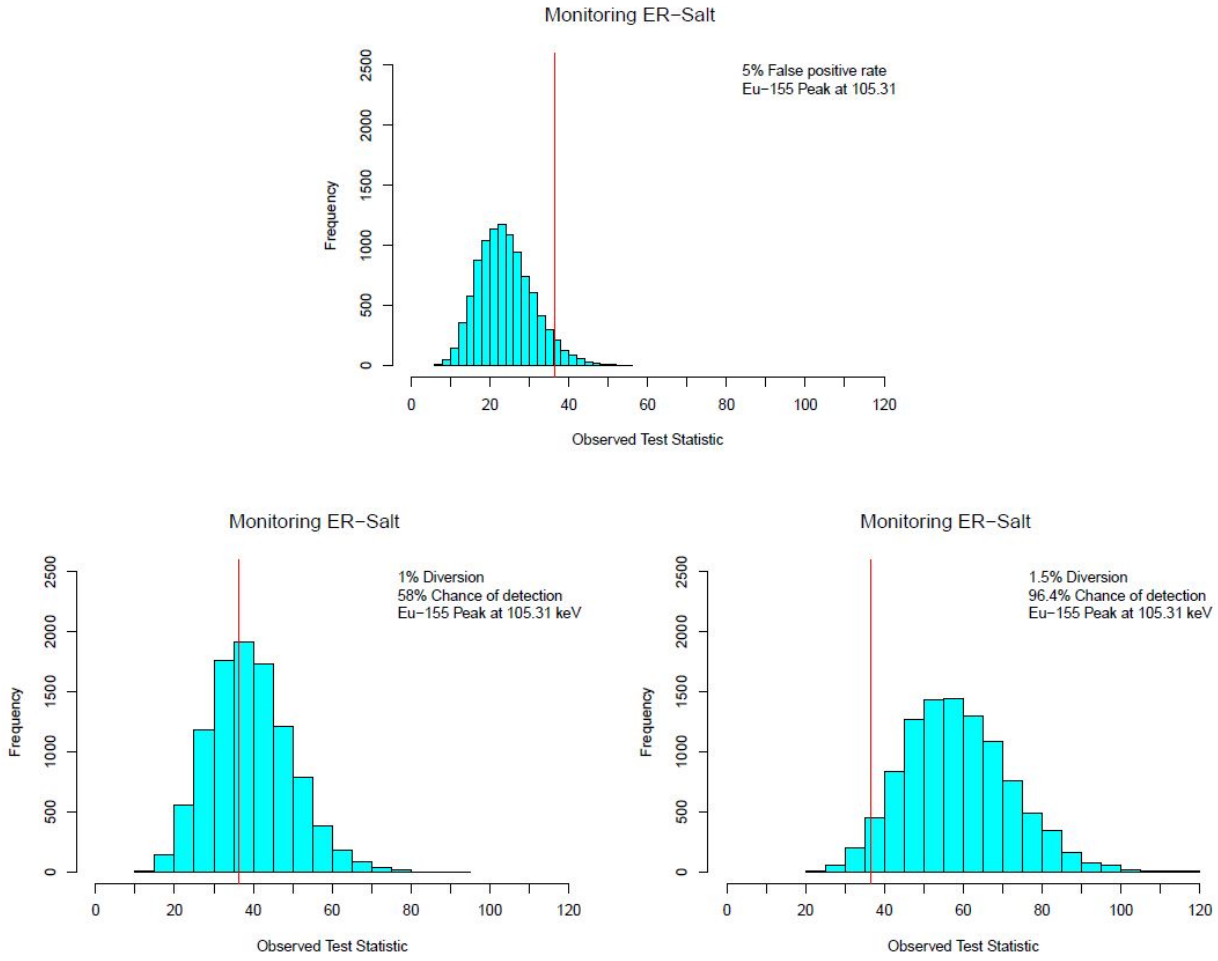

Figure 6: Monitoring ER-salt with Eu-155 counts at 105.31 keV

8 Micro-Calorimeter Spectra for Source Term

Figure 7 shows ten high intensity gamma peaks from the source term. For almost all of the isotopes, it's hard to tell what energy bin contains the "peak". If a peak can't be clearly defined then it will be hard to use that peak for detecting a diversion using the micorcalorimeter.

For illustration consider the data in the top panel of Figure 8. The Np-239 peak is supposed to be at 106.12 keV and there are two high counts near this energy. How many data points on each side of 106.12 actually belong to the peak is hard to say and including data that is essentially just noise is going to lower the detection probability.

The bottom plots in Figure 8 shows detection probabilities for two scenarios. For both scenarios the signal is between 106.06 and 106.18, which corresponds to the data between the blue lines in the top panel. The bottom left plot shows a histogram of values of the test statistic when we include noise data from 105.8 to 106.44 (solid black lines). The probability of detecting a diversion is about 32%. The bottom right plot is similar but we only include noise data from 106.02 to 106.22 (dashed black lines). The probability of detecting a diversion is now about 59%. This illustrates the importance of being able to define the regions of interest when determining detection probabilities for the microcalorimeter.

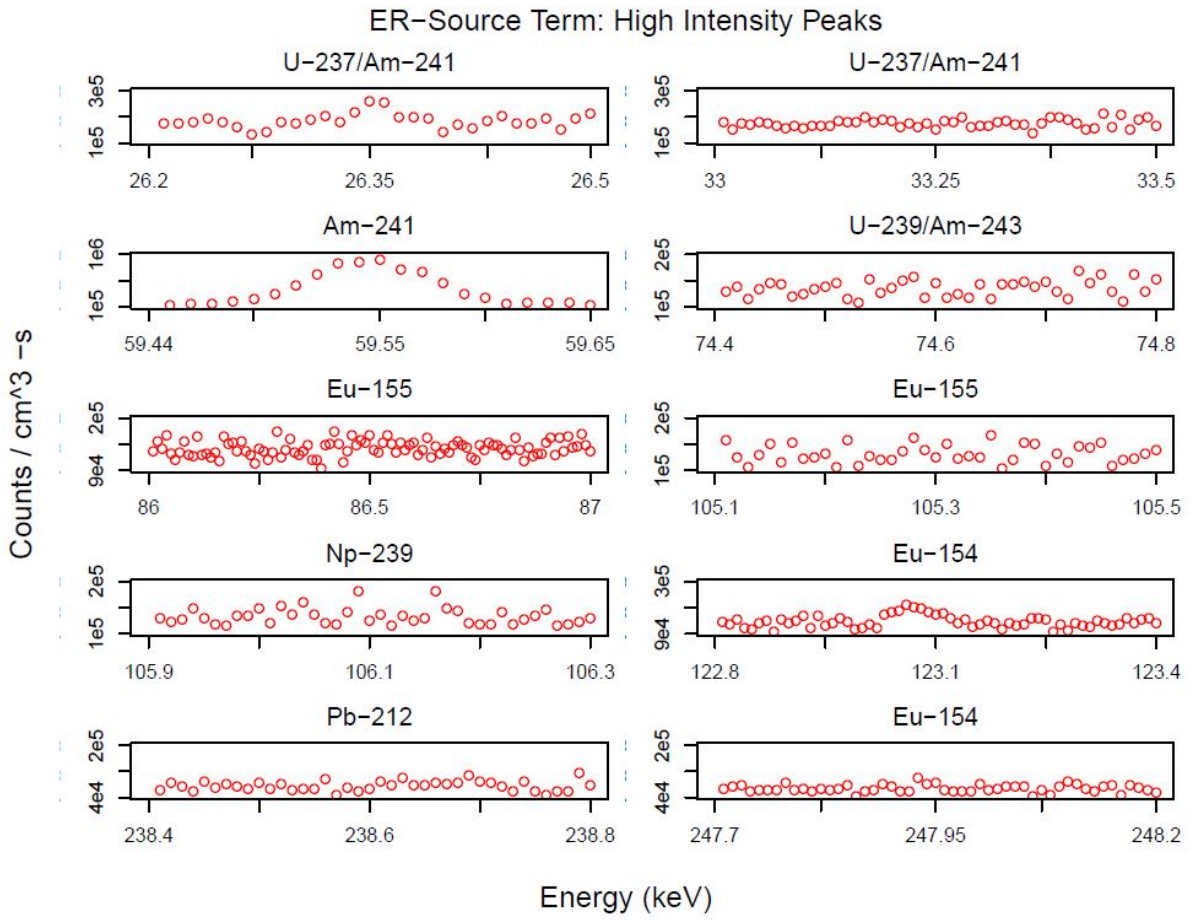

Figure 7: ER source term isotopes of interest.

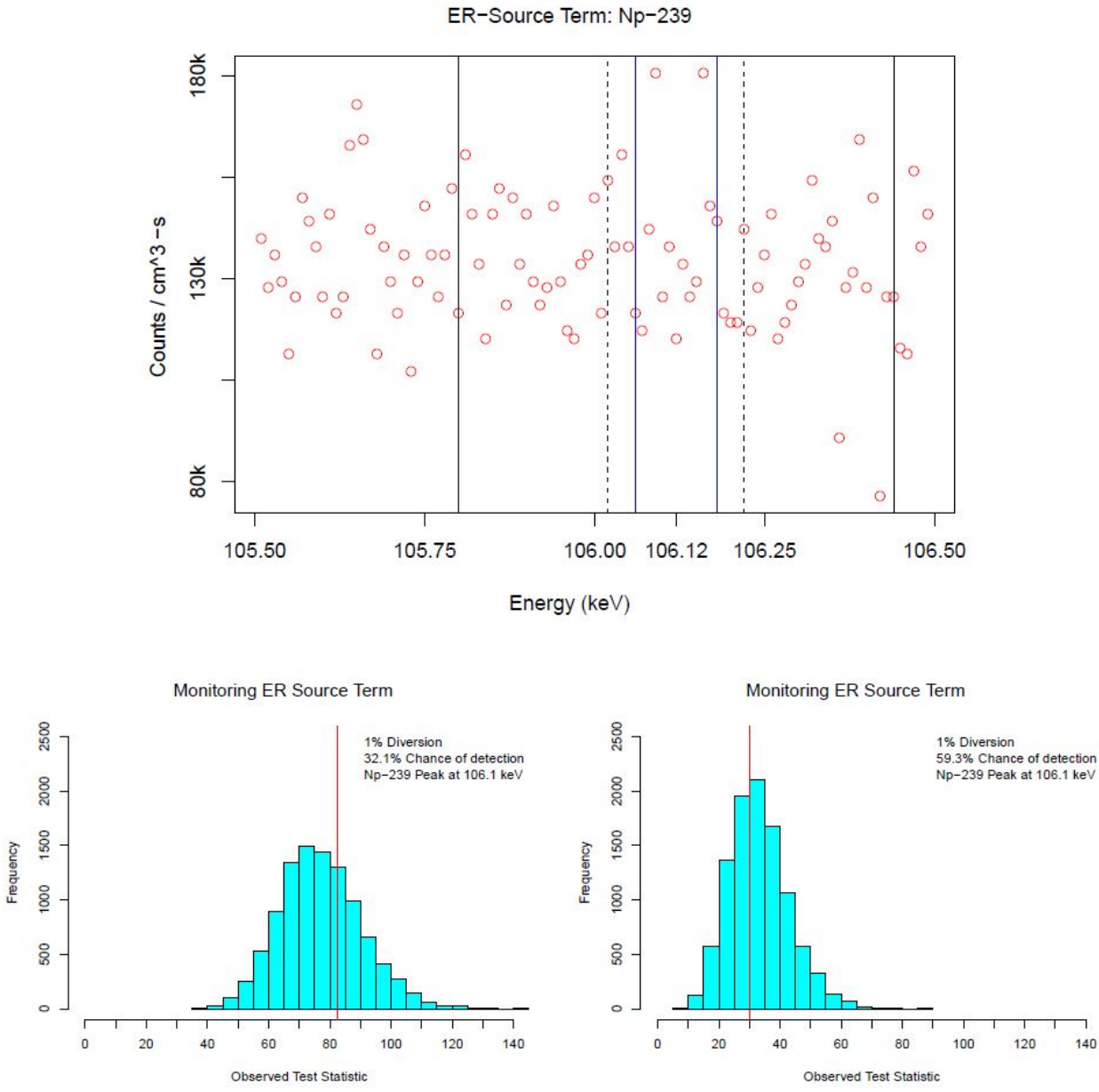

Figure 8: Top panel shows data around the Np-239 peak at 106.12. To estimate a probability of detection (PD) we defined the signal to be between 106.06 and 106.18 (solid blue lines). The bottom left panel shows the PD when we include noisy counts between the solid black lines and the blue lines. The bottom right panel shows the PD when the noisy counts are between the dashed black lines and the blue lines.

9 Voltammetry

At the conclusion of this year, the advanced integration team began working with the Voltammetry team from ANL. Initial results were generated that still need to have statistical integration done to determine the performance of the voltammetry sensor. This section highlights the data we have received. Elemental mass data from the SSPM model was sent to the Voltammetry technology development team at ANL. With this data they were able to simulate the response of their voltammetry sensor to several ER salt compositions. The response of the voltammetry sensor is shown as the bold black line in Figure 9. The contributions of different species are also shown in the figure with dotted lines.

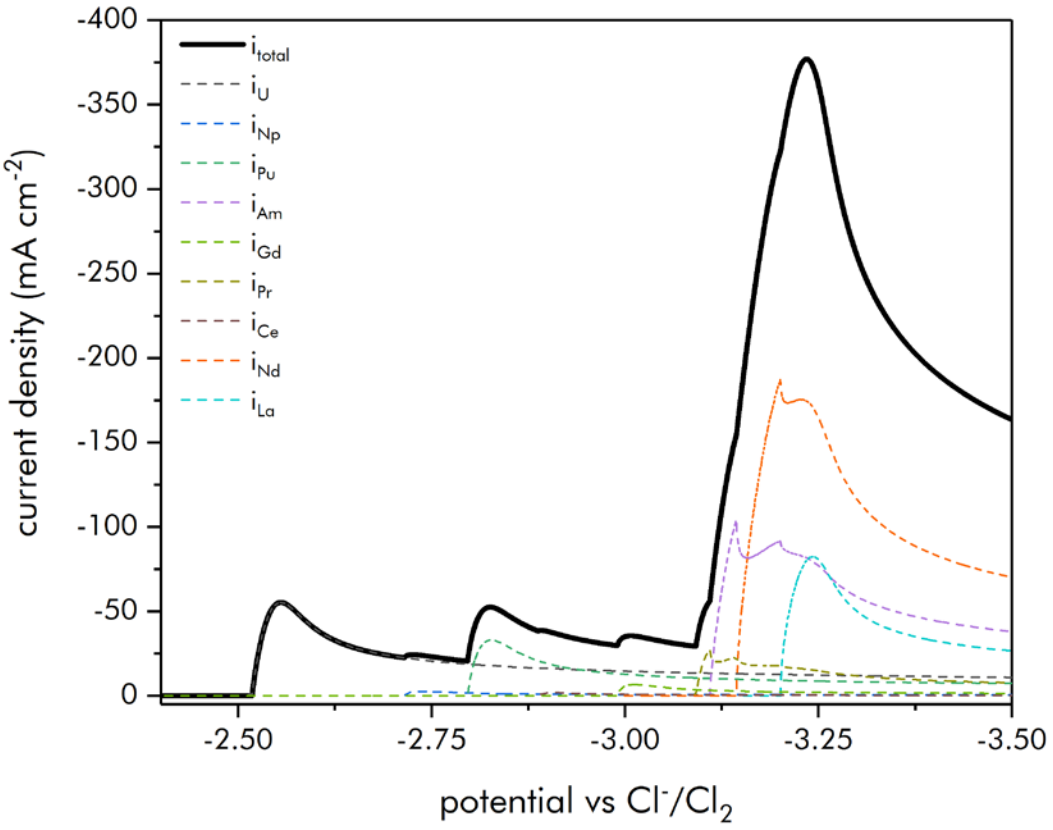

Figure 9: Voltammetry response to ER salt composition (data and figure courtesy of N. Hoyt – ANL).

Three more simulations were requested that represented a reduction of 1%, 5%, and 10% plutonium concentration in the salt. Figure 10 shows a plot of the region associated with the plutonium peak and displays the effect of decreasing the plutonium concentration in the salt on the waveform.

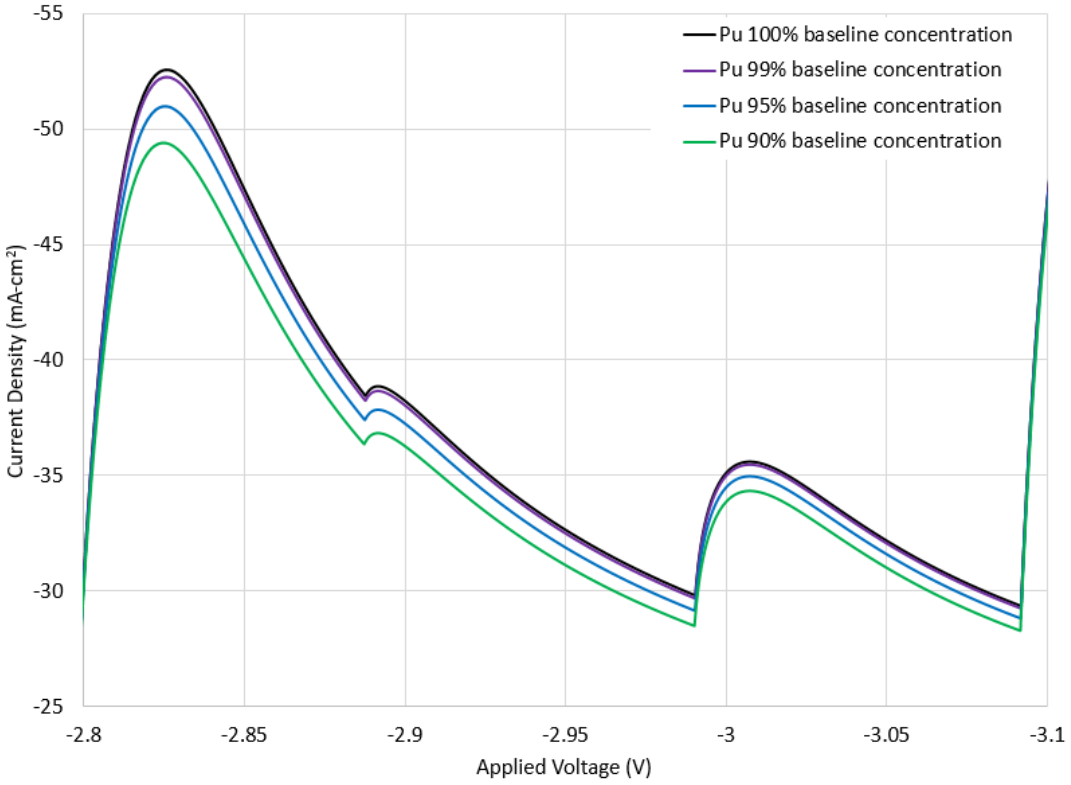

Figure 10: Changes in voltammetry waveform as a result of reduced plutonium concentrations in the ER salt (data courtesy of N. Hoyt – ANL).

Currently, as of the writing of this report, work is on-going to interpret the results presented in Figures 9 and 10. Future reporting will include results from this data.

10 Conclusions

We have successfully demonstrated advanced integration methods for incorporating the HDND and microcalorimeter MPACT sensor technology for detection near an electrorefiner. The methods have been calibrated with an agreed upon flowsheet from SSPM provided by SNL. General conclusions can be made regarding the performance of the HDND and microcalorimeter including but not limited to: The HDND has been shown to be highly effective at the specified locations to check U product and U/TRU product for Pu diversions of relatively small amounts of Pu. The microcalorimeter is good at detecting small diversions using intense peaks in the spectrum as the statistical data point. Elements such as Americium, Curium, Uranium and Neptunium are good indicators only if the peaks standout in the spectrum. Large peaks such as Eu-155, Am-241, Eu-154, and U-239/Am-243 may be utilized for detection once better isotopic data is known as well as understanding how these isotopes change according to diversions. These determinations were made based on the variability in counting statistics and future work will need to account for other sources of uncertainty. Future work will include advanced integration methods used at exploring additional MPACT developed sensor technologies, such as the Voltammetry detector and microfluidic sampler.

References

1. Cipiti, Benjamin B., et al. “Modeling and Design of Integrated Safeguards and Security for an Electrochemical Reprocessing Facility” Sandi Report, SAND2012-9303 (2012).

2. Wilson, W. B., et al. “SOURCES 4C: A Code for calculating (α,n), Spontaneous Fission, and Delayed Neutron Sources and Spectra” Proc. of the Radiation Protection and Shielding 12th Biennial Topical Meeting, Santa Fe, NM April 14-18 (2002)

3. C.J. Werner(editor), "MCNP Users Manual - Code Version 6.2", Los Alamos National Laboratory, report LA-UR-17-29981 (2017).

4. Tutt, J. R., McKinney, G. W., Wilcox, T. A., “All-Particle Spontaneous-Decay and Delayed-Positron Capabilities in MCNP6”, Proc. of the American Nuclear Society ANTPC, Santa Fe, NM September 27th (2016).

5. Henzlova, D., Menlove, H. O., “High-Dose Neutron Detector Development for Measuring Alternative Fuel Cycle Materials”, Proc. of GLOBAL 2017, Seoul, Korea September 24-29 (2017).

6. Hoover, A. S., et al. “Determination of Plutonium Isotopic Content by Microcalorimeter Gamma-Ray Spectroscopy”, IEEE Transactions on Nuclear Science, Vol. 60, No. 2, April (2012).

7. Key, B. P., et al. “Advanced Integration Methods for Monitoring an Electrorefining Process”, Los Alamos National Laboratory, report LA-CP-18-20204 (2018).

8. Solomon, C. J., “The Intrinsic Source Constructor Package: Installation and Use”, Los Alamos National Laboratory, report LA-UR-12-22234 (2017).

9. Agostinelli, S., et al. “Geant4 – a simulation toolkit,” Nucl. Instrum. Meth. Phys. Res., vol. A 506, pp. 250-303, (2003).